

Evaluation of `Photos` Monte Carlo ambiguities in case of four fermion final states

A. Kusina^a and Z. Was^b

Institute of Nuclear Physics Polish Academy of Sciences, PL-31342 Krakow, Poland

Received: date / Revised version: date

Abstract. With the increasing precision requirements and growing spectrum of applications of Monte Carlo simulations the evaluation of different components of such simulations and their systematic ambiguities become of utmost interest. In the following, we will address the question of systematic errors for `Photos` Monte Carlo for simulation of bremsstrahlung corrections in final states, which can not, in principle, be identified as a decay of resonances. It is possible, because the program features explicit and exact parametrization of phase space for multi-body plus multi-photon final states. The `Photos` emission kernel for some processes consist of complete matrix element, in the remaining cases appropriate approximation is used. Comparisons with results of simulations, from generators based on exact phase space and exact fixed order matrix elements, can be used. For the purpose of such validations `Photos` provides an option to restrict emissions to single photon only. In the current work we concentrate on final state bremsstrahlung in $q\bar{q}(e^+e^-) \rightarrow l^+l^-l^+l^-\gamma$ and $\gamma\gamma \rightarrow l^+l^-\gamma$ processes. The reference distributions used as a cross-check are obtained from the fixed-order `MadGraph` Monte Carlo simulations. For the purpose of validation we concentrate on those phase space regions where `Photos` is not expected to work on the basis of its design alone. These phase space regions of hard, non-collinear photons, do not contribute to large logarithmic terms. We find that in these phase space regions the differences between `Photos` and `MadGraph` results do not surpass a few percent and these regions, in turn, contribute about 10% to the observed process rates. This is encouraging in view of the possible ambiguities for precise calculation of realistic observables.

Contents

1	Introduction	1
2	Details of samples used for validation	2
2.1	$q\bar{q} \rightarrow l^+l^-l^+l^-(\gamma)$ process	2
2.2	$\gamma\gamma \rightarrow l^+l^-(\gamma)$ process	3
3	Results	3
3.1	Case of four lepton final states	3
3.1.1	$q\bar{q} \rightarrow \mu^+\mu^-\tau^+\tau^-(\gamma)$	5
3.1.2	$q\bar{q} \rightarrow \mu^+\mu^-\mu^+\mu^-(\gamma)$	6
3.1.3	$q\bar{q} \rightarrow \tau^+\tau^-\tau^+\tau^-(\gamma)$ at $\sqrt{s} = 10.5$ GeV	7
3.2	Case of $\gamma\gamma \rightarrow l^+l^-(\gamma)$	8
4	Usage for phenomenology	8
5	Summary	9
A	Details on running <code>MadGraph</code> and kinematic cuts	12
B	Technical comparison plots for $q\bar{q} \rightarrow \gamma\mu^+\mu^+\mu^-\mu^-$ at different energies	13
B.1	MC-tester: $q\bar{q} \rightarrow \gamma\mu^+\mu^+\mu^-\mu^-$ at $\sqrt{s} = 125$ GeV	13
B.2	MC-tester: $q\bar{q} \rightarrow \gamma\mu^+\mu^+\mu^-\mu^-$ at $\sqrt{s} = 150$ GeV	17
B.3	MC-tester: $q\bar{q} \rightarrow \gamma\mu^+\mu^+\mu^-\mu^-$ at $\sqrt{s} = 240$ GeV	21

1 Introduction

Phenomenology of High Energy Physics experiments require careful comparison of experimental results with theoretical predictions. An agreement between the two represents confirmation

of the current theory and calculational schemes, a discrepancy on the other hand can be an indicator of New Physics phenomena or point to inadequacy of the applied approximations. For that purpose, all elements of theoretical predictions and detector responses, need to be reviewed whenever new threshold of sophistication is reached. Each element of the predictions as well as the strategy of combining the individual parts need to be validated anew.

It is generally believed that Monte Carlo simulations offer feasible solution whenever all theoretical and experimental effects need to be taken into account simultaneously. Electroweak effects can be defined as separate part of such simulation systems. Recently, we have evaluated numerically if such separation scheme developed in LEP times still holds in phenomenology of Dell-Yan processes for present day applications [1]. See there for further references, in particular, on the fundamental result enabling the separation of the electroweak effects into separate parts. Here we concentrate on QED final state radiations in processes of four-lepton final states produced in high energy e^+e^- or pp collisions as well as $\gamma\gamma \rightarrow l^+l^-$ hard processes. In such cases precision requirements are lower, nonetheless recently an interest for such predictions arise, see e.g. [2]. The separation of the QED effects from the complete electroweak effects does not seem to be the precision obstacle, nor dividing the QED contributions into parts; one of them the final state radiation.

In the present paper, we address the adequacy of `Photos` Monte Carlo [3,4] for final state photon radiation in $e^+e^-(q\bar{q}) \rightarrow$

^a e-mail: aleksander.kusina@ifj.edu.pl

^b e-mail: zbigniew.was@ifj.edu.pl

$l^+l^-l^+l^-(n\gamma)$ and $\gamma\gamma \rightarrow l^+l^-(n\gamma)$ processes. These processes are outside of the default *Photos* applicability domain. However, predictions for them can be obtained from different Standard Model calculations [5–10]. Therefore, for the validation of *Photos* in this region one does not need to rely on comparisons with the data. At the same time *Photos* is very valuable as it can be combined with calculations/simulations enabling higher order corrections and flexible acceptance cuts providing complete calculations assuring control of technical aspects, resummations, technical cuts used to separate phase space regions of singularities. This can be done because of its design and algorithm modifying events stored already in event records. Fortunately the lowest order processes and processes with added photons, are implemented e.g. in *MadGraph* [5] and can be used for phase space regions where predictions of *Photos* require validation.

Crude level *Photos* Monte Carlo algorithm is non-Markovian. The event to which photons may be added, is first read from the event record produced by other program, then the momenta coordinates are calculated back, using specifically chosen parametrization. These variables are used for parametrization of phase space slots were additional photons are added. The number of photon candidates is generated from Poissonian (or binomial) distribution. For each photon, to be constructed, the variables are generated. They are used to complete phase space parametrization for the new configuration with additional photons. At this step, no energy momentum conservation is enforced, Jacobians of phase space parametrization are absent as well as emission kernels representing approximated or interpolated matrix elements. They are introduced later with weights and rejection of photon candidates through iterative algorithm.¹ If construction of the photon is rejected, previous kinematic configuration is retained. For rejection we rely on Kinoshita-Lee-Nauenberg theorem [11, 12]. Only numerically minor, process dependent, corrections need further care if complete first order QED matrix element is used. The details of event generation in *Photos* are explained in [4, 13], phase space parametrization is possibly best described in [14]. What is important is that the algorithm covers the full multi-photon phase space and parametrization is exact, whenever it is necessary. This means that approximations for the phase space always match those of matrix element.²

For the sake of universality, since ref. [13], simplified kernel with respect to the exact first order matrix element was used for all processes and multi-photon radiations. However, already then, interference effects for emissions from all final state charges were introduced and good agreement with (matrix element based) reference simulations was achieved. This, distinct from parton shower approach enabled rigorous introduction of exact matrix elements which was done in certain two-body decays including: Z/γ^* [16], W, γ^* [17] and K^*, B^* [14].

Now we turn our attention to final state photon radiation in $q\bar{q} \rightarrow l^+l^-l^+l^-(n\gamma)$ and $\gamma\gamma \rightarrow l^+l^-$ processes and specially to *Photos* ambiguity for these cases.

¹ This sometimes leads to confusion and misinterpretation of the algorithm design as Markovian of shower type which it is not.

² When testing algorithm for Z decays, using $Z \rightarrow l^+l^-n\gamma$ matrix elements, it was found that phase space approximations related to the combination of generation of parallel presamplers and implementation of interference weight should match those of matrix element [15].

The remaining part of the paper is organized as follows. In Sec. 2 we provide details on the samples used for tests with certain more technical details delegated to appendix A. Section 3.1 is devoted to validation of *Photos* for $q\bar{q}(e^+e^-) \rightarrow l^+l^-l^+l^-(n\gamma)$ process and Sec. 3.2 for the $\gamma\gamma \rightarrow l^+l^-$ process. Section 4 discusses *Photos* usecases and its interfacing with other programs. The obtained results are summarized in Sec. 5. Additionally, appendix B collects numerical results automatically obtained with the help of the *MC-tester* program [18].

2 Details of samples used for validation

In order to perform validation of *Photos* in the new kinematic domain discussed earlier we use the following approach. For each of the considered processes (e.g. $q\bar{q} \rightarrow l^+l^-l^+l^-$) we use *MadGraph* to generate two samples: first for a base process without any photons in the final state, and second for an analogous process but with one additional photon in the final state. Then the first sample is supplemented with additional photon generated using *Photos*. This is possible because of the special single photon emission mode of *Photos*. Typically we use samples (after selection cuts) of around 50000 events with photons. In the next step distributions calculated from the two samples (*MadGraph* with additional photon and *MadGraph* supplemented by photon from *Photos*) are compared. Histograms of all possible invariant masses which can be build from the final state momenta are constructed and then compared. That simplifies the first step of tests. For the actual study of ambiguity for observables of phenomenological merit the appropriate selection cuts, which are as close as possible to the realistic ones, should be used. Only then systematic ambiguity can be obtained with sufficient certainty.

The kinematic selection cuts play here an additional more technical role. The event simulation with *MadGraph* is best suited for generation of configurations, where there is a separation between the outgoing particles. That is why cuts on distance, ΔR , between final state particles, and minimal energy of the final state photon, E_γ , are always used. In this way non-interesting for tests of *Photos*, but difficult for *MadGraph*, phase space region of infrared and/or collinear singularities is avoided. Fortunately in those collinear and infrared regions *Photos* does not need to be re-tested.

In the following we discuss separately the details of samples generated for the two considered types of processes.

2.1 $q\bar{q} \rightarrow l^+l^-l^+l^-(\gamma)$ process

For the $q\bar{q} \rightarrow l^+l^-l^+l^-(\gamma)$ process we have generated three sets of samples for different center of mass energies: $\sqrt{s} = \{125, 150, 240\}$ GeV (each set consisted of a process with and without a photon in the final state). The selection of Feynman diagrams entering such calculations are shown in Figs. 1 and 2 correspondingly for process without and with the final state photon. Additionally, one should note one more important detail. When generating *MadGraph* samples for processes with additional final state photon we wanted to add the photon only in the final state. As a consequence we needed to remove some of the diagrams from *MadGraph* calculations. Specifically, we

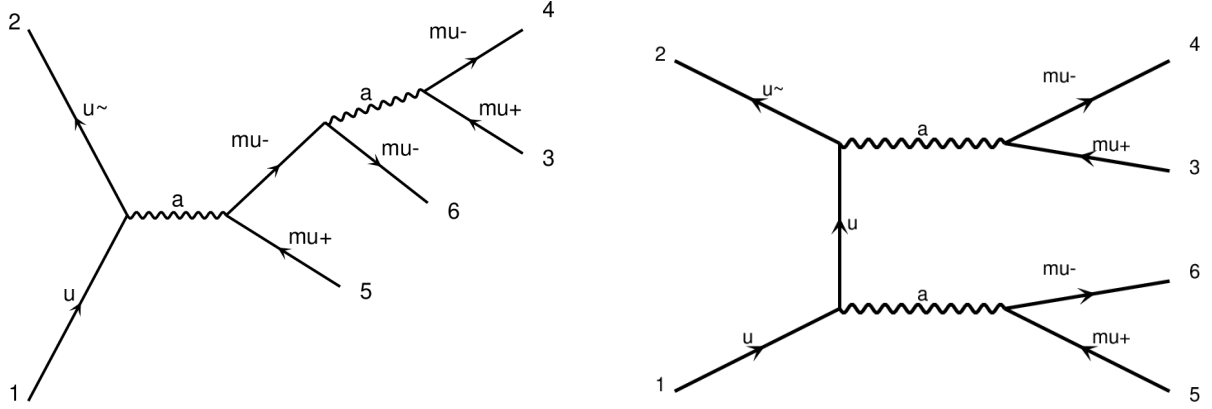


Fig. 1: Typical diagrams contributing to the amplitude of $q\bar{q} \rightarrow \mu^+\mu^-\mu^+\mu^-$ production. Note that a stands here for either photon or Z boson.

removed diagrams where photon was radiated from the initial state quarks as well from the t -channel intermediate quark, example diagrams of this kind are displayed in Fig. 3. In this way we were left with a gauge invariant subset of diagrams yielding a sensible result which in turn could be directly compared with the MadGraph sample supplemented with photon added from *Photos*.³

For all these samples the kinematic selection cuts used in MadGraph were always the same (with additional isolation cuts on the final state photon if present). We tried to keep them as wide as possible but taking care not to spoil the convergence of the calculation. That way we allowed ourselves an option to further restrict the cuts later on after including additional photon from *Photos*. This can be useful as more restrictive cuts on the MadGraph sample without the final state photon could, due to the kinematics, restrict the possibility of generating the additional photon with *Photos*.

The specific values used for kinematic selection cuts are listed below, we also provide an example MadGraph input file (run card) in App. A. One should note that the same cuts for the photons were applied independently of whether the photon was generated from MadGraph or added later with the help of *Photos*. Also the electroweak initialization parameters for the compared two cases were taken the same.

1. Maximal rapidity of individual charged leptons: $|\eta_l| < 3$.
2. Minimal invariant mass of same flavor and opposite charge lepton pairs: $m_{l+l-} > 9 \text{ GeV}$.
3. Minimal distance between final state leptons: $\Delta R_{ll} > 0.4$.
4. Maximal rapidity of final state photons: $|\eta_\gamma| < 3$.
5. Minimal energy of final state photons: $E_\gamma > 5 \text{ GeV}$.
6. Distance between final state photon and each lepton: $\Delta R_{l\gamma} > 0.4$.
7. Transverse energy: $E_t < \frac{1-\cos(\Delta R_{l\gamma})}{1-r_0^\gamma} \sqrt{(p_\gamma^1)^2 + (p_\gamma^2)^2}$, with $r_0^\gamma = 0.4$.

The definitions of kinematic variables used for constructing the above kinematic cuts are provided in App. A.

³ On the technical level this was achieved by invoking a user defined `diagram_filter` function. We would like to thank Richard Ruiz and Olivier Mattelaer for help in doing this.

2.2 $\gamma\gamma \rightarrow l^+l^-(\gamma)$ process

For the $\gamma\gamma \rightarrow l^+l^-(\gamma)$ process we have generated two MadGraph samples: one for the process without the photon in the final state and one with the additional photon, both samples were generated at center of mass energy of $\sqrt{s} = 125 \text{ GeV}$; both comprise of 40000 events. Example Feynman diagrams contributing to the calculation of the $\gamma\gamma \rightarrow l^+l^-(\gamma)$ process are displayed in Fig. 4.

The kinematic cuts used for these processes were the same as for the process $q\bar{q} \rightarrow l^+l^-l^+l^-(\gamma)$ with the simplification that there was no need to subselect diagrams that enter MadGraph calculation with extra photon. Again the MadGraph sample without final state photon was supplemented with a photon generated using *Photos* and the two were compared.

3 Results

For the purpose of validation we have chosen two sets of processes, first the $q\bar{q} \rightarrow l^+l^-l^+l^-(\gamma)$ and later the $\gamma\gamma \rightarrow l^+l^-(\gamma)$ which turned out to be simpler. We should note that the results shown for the $q\bar{q} \rightarrow l^+l^-l^+l^-(\gamma)$ process holds with nearly no alteration for the process where quarks are replaced by electrons $e^+e^- \rightarrow l^+l^-l^+l^-(\gamma)$. Such process was also checked but we will not show explicit results for it here.

In order to simplify the comparisons and also to obtain a better understanding we have staged the performed tests. This is especially true for the case of four lepton production process. In what follows we will discuss the different stages but will present explicit numerical results only for the most important parts.

We note that options of *Photos* initializations, such as activation of interference effects, single or multiple photon mode of operation are carefully explained in the program manual, ref. [4].

3.1 Case of four lepton final states

The algorithm of *Photos* use explicit phase space parametrization, also part of the emission kernel originating from matrix element is explicitly coded. It is thus possible to install exact,

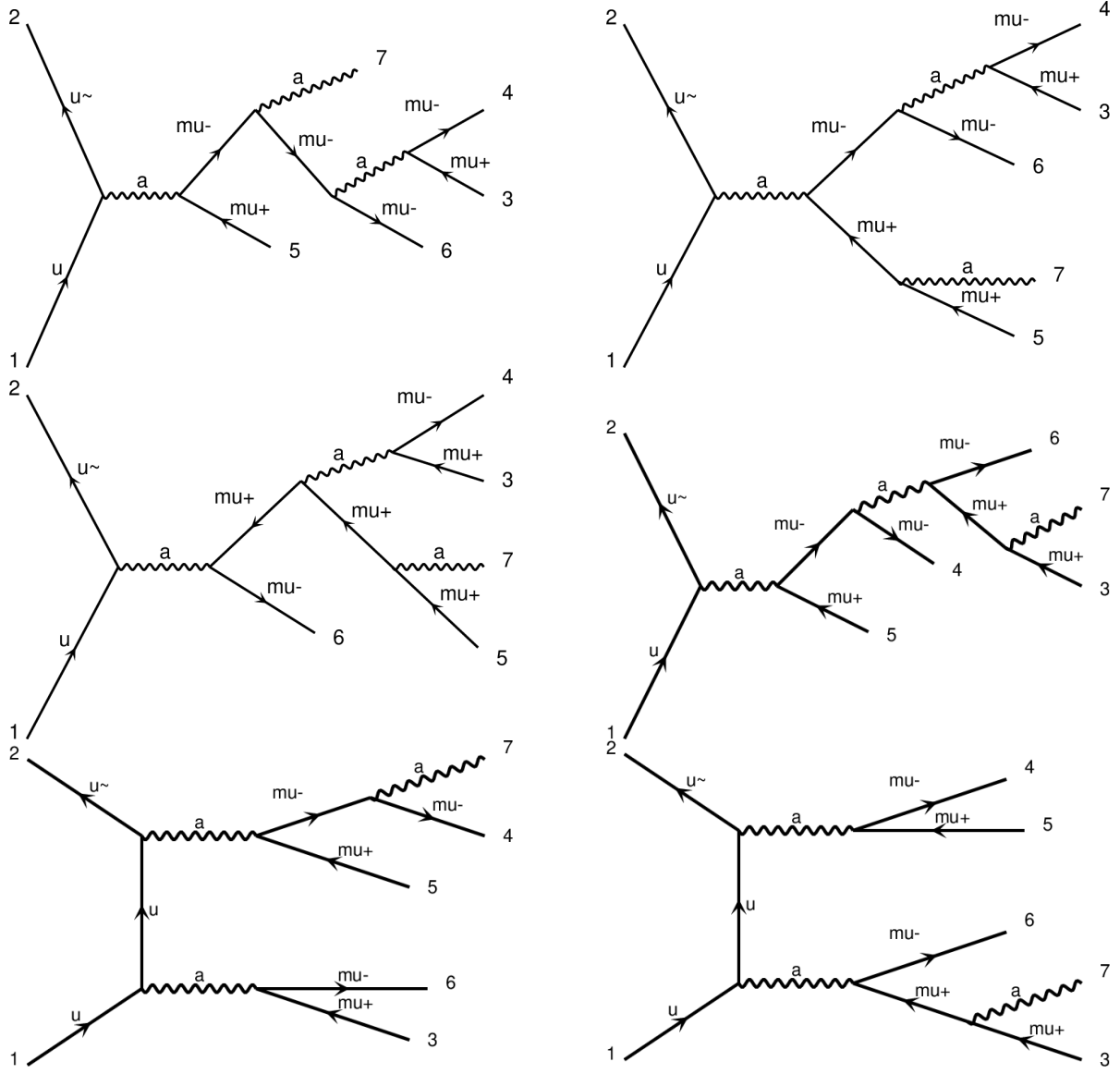


Fig. 2: Typical diagrams contributing to the amplitude of $q\bar{q} \rightarrow \mu^+\mu^-\mu^+\mu^-\gamma$ production. Note that a stands here for either photon or Z boson.

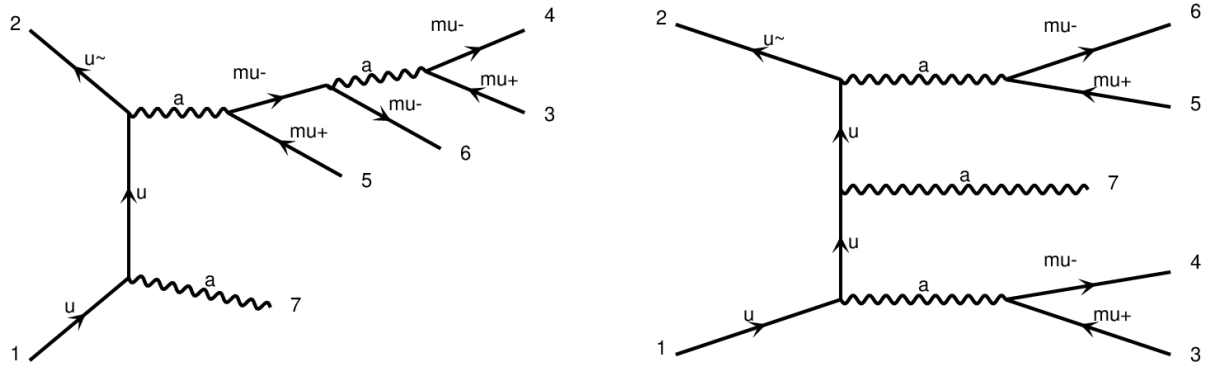


Fig. 3: Typical diagrams with photon radiation in the initial state or from the t -channel which were removed from MadGraph calculations of $q\bar{q} \rightarrow \mu^+\mu^-\mu^+\mu^-\gamma$ process. Note that a stands here for either photon or Z boson.

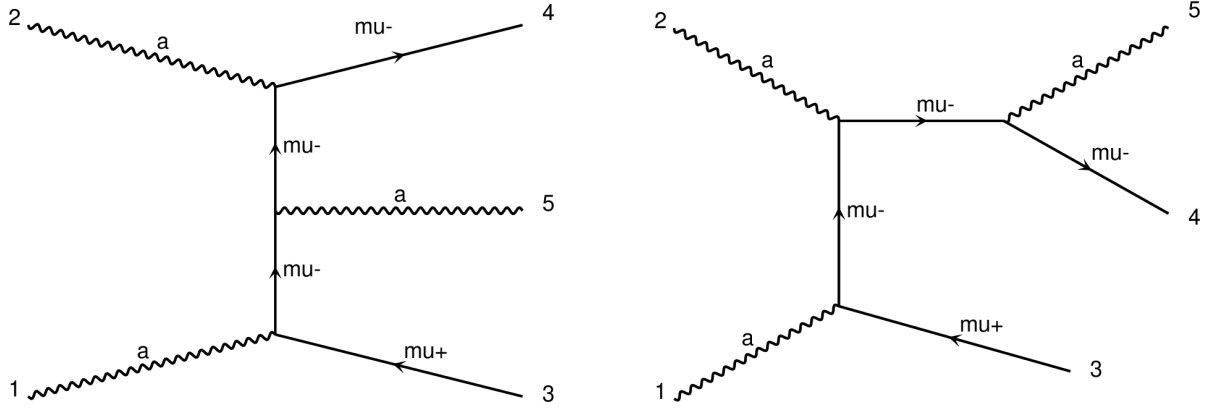


Fig. 4: Diagrams contributing to amplitude of $\gamma\gamma \rightarrow \mu^+\mu^-\gamma$ production. Note that a stands here for photon only.

single photon emission matrix element and improve quality of generation. That was implemented for several two body final states.

For the four fermions final state like $l^+l^-l^+l^-$, until now, there were no matrix elements installed into public version of *Photos* emission kernel. In principle, it is possible and in fact such kernel, was temporarily installed for emission of lepton pairs in case of $Z \rightarrow l^+l^-$ (l^+l^-) that is for lepton pair emission instead of bremsstrahlung photons, see refs. [19,20]. In that case four body phase space was elaborated and exact parametrization was used. It turned out, that approximate form of matrix element used for emission kernel, was sufficient for quite impressive precision. An approximation better than the eikonal one of ref. [21] was developed. Now we investigate if the same level of accuracy can be achieved for final state bremsstrahlung and processes like $q\bar{q} \rightarrow l^+l^-l^+l^-\gamma$. One could think of such process as production and decay of the Z-boson pair, but this weakens assumptions, especially for energies which are insufficient for the on shell two-boson state formation. In case of four (same flavor) fermion final states, more than two resonant configuration may simultaneously contribute and complicate the input for *Photos*. For such processes tests are required. The case is at the edge of program applicability domain.

When testing *Photos* for the case of process with four lepton final states we did the following steps:

1. Consider final states where two pairs of leptons carry different flavors.
2. Require certain number of intermediate Z-bosons.
3. Test different initialization options + interferences.
4. Consider different center of mass energies.
5. Investigate the most complex production of four (same flavor) leptons including the γ/Z interferences.

3.1.1 $q\bar{q} \rightarrow \mu^+\mu^-\tau^+\tau^-(\gamma)$

We have started our tests with a simple case of $q\bar{q} \rightarrow ZZ \rightarrow \mu^+\mu^-\tau^+\tau^-(\gamma)$ process. Also the mass of τ lepton was reduced to the one of the muon. That way the number of interferences and contributing diagrams was much smaller than for the four muon production. Once the intermediate bosons were explicitly written into the event record, the agreement between *MadGraph*

and *Photos* was perfect.⁴ Comparisons were prepared with help of the *MC-tester* [18] program. All possible invariant masses which can be formed from momenta of the outgoing particles were monitored, but not multidimensional distributions.

For the $\mu^+\mu^-\tau^+\tau^-$ (later also for the four muon final states) several options of *Photos* initialization settings were investigated. Interference effects in *Photos* between emissions from $\mu^+\mu^-$ and $\tau^+\tau^-$ pairs were switched on and off. For that purpose, intermediate *Z* bosons (alternatively none or just one) were explicitly present/absent in the event record before call to *Photos*. It was found that at very high energies the interference between emission amplitudes for two *Z* bosons forming lepton pairs are small. However, at lower energies when *Z* bosons are not ultra-relativistic, emission interferences are not so much reduced by the directions of leptons and the resulting separation of the emission dipoles. As a result the *Z* peak constraint has to be taken into account explicitly.

In the first run of tests, the final state fermions were of different flavor to minimize number of diagrams contributing to *MadGraph* amplitudes. At 240 GeV agreement was reasonable, but no *s*-channel photon exchange was taken into account. Production takes place above *ZZ* threshold so clearly two *Z* resonant contribution dominates and such intermediate states were written into event record to simplify the task for *Photos* algorithm. Two independent, two body *Z* decays were processed. Then, second round of tests were performed. The only modification was that center of mass energy was reduced to 150 GeV. Thus one of the *Z* bosons must have been off the resonance peak. Still no *s*-channel photon exchange was taken into account. Further reduction of center of mass energy did not introduce any changes or concerns.

In our following tests with center-of-mass system energy in 125-240 GeV range the agreement with *MadGraph* simulations, seem to be optimal when lepton pair of virtuality closest to the *Z* mass was written in the event record as originating from the intermediate *Z* boson (written explicitly into event record). If both possible lepton pairs virtualities were more than 3-4 GeV away from the *Z* virtuality, the intermediate bosons were not written into the event record. Similar arrangements for small lepton pair virtualities (when exchange of virtual photon was taken into account) was not helpful/necessary, possibly because of the applied cuts, excluding such phase space regions.

Finally we have found, that if the interference effects were active in *Photos* and intermediate bosons were explicitly written the agreement was reasonable for all numerical results of standard tests for all one-dimensional invariant mass distributions.

3.1.2 $q\bar{q} \rightarrow \mu^+\mu^-\mu^+\mu^-(\gamma)$

Encouraged by the positive results of the tests described above, we have moved to the next step: the four muon final states. We

⁴ Since by default *Photos* assumes nearly flat distributions the efficiency of the algorithm drops when encountering resonances. Because of this we need to inform *Photos* about the presence of the resonance which is done by introducing such intermediate states into the event record produced with *MadGraph*.

have taken into account the *s*-channel photon exchange too.⁵ Typical diagrams contributing to this process are collected in Sec. 2.1

The results of these technical tests are collected in Appendices B.1-B.3 for center of mass energies of {125, 150, 240} GeV. In these cases the obtained agreement may look not that impressive, as the differences of the normalized area under the one dimensional histograms of up to 5% were found. However, one should not forget that these histograms were constructed from events where only hard, non-collinear, photons were taken, that is from about 10% of the accepted events. For 90% of events, either no bremsstrahlung photons were present, or they were soft and/or collinear. For such cases *Photos* algorithm performs accurately thanks to its design, that is why, such regions of the phase space were not included in the test distributions as they do not contribute to ambiguities. Naively this would point to a tiny ambiguity of the order ~ 0.005 . In reality the differences may be even smaller, as the use of *Photos* distorts original order of particles and the first and second occurrence of e.g. μ^+ may feature different distribution.⁶ This may be observed from our Fig. 5 for $\mu^+\mu^-$ invariant mass and Fig. 6 for $\mu^+\mu^-\gamma$.⁷

Now, the *s*-channel photon exchange is taken into account. Also, the four muons in the final state imply, that the *Z* resonance can be formed from four combinations of leptons. The pattern of interferences and intermediate resonances, may be more challenging for the *Photos* algorithm to include.

For the highest center of mass energy of 240 GeV the virtuality of the system is above the threshold for the pair of *Z* boson production. As a consequence, in order to achieve agreement, we have to call *Photos* for the *Z* decays separately. This prevents the algorithm to ignore the *Z* peak constraint on distributions. Additionally, we have to order momenta, prior to invoking *Photos*, so the first pair of muons would be closest to the *Z* peak. If the pair could be within ± 3 GeV from the *Z* peak, we write the *Z* into the event record prior to invoking *Photos*. As a consequence its algorithm will not deform the shape of the intermediate resonance peak, but at the same time interferences of emissions from all four muons will be reduced to interferences within the two separate $\mu^+\mu^-$ pairs. This seems not to be physical if none of the muon pairs is originating from the resonance peak. Such interface to *Photos* clearly leads to temporary ordering in the events with identical muons. This ordering could make the interpretation of the comparisons pro-

⁵ Depending on the choice, the Feynman diagrams with *s*-channel photon exchange were taken into account, or not, both in four lepton and four lepton plus final state photon samples, generated by *MadGraph*.

⁶ For the case of $\mu^+\mu^+\mu^-\mu^-$ final state pair of intermediate *Z* bosons contribute. There are two interfering diagrams depending on how identical muon pairs are attributed to bosons. This has consequences not only for *Photos* interface and its ambiguities but also for the technicality of the tests. In principle, we could have symmetrize randomly position of same charge muons before our testing program *MC-tester* [18] is invoked. *MC-tester* is sensitive to how identical particles are ordered in the event record. This artefact of our tests slightly increase the differences seen in the test results. However, since results are anyway sufficiently good, we have not investigated at this time, how large is the resulting increase of the ambiguity.

⁷ The *y*-axis of Fig. 5 (and later plots) shows the number of events normalized in such a way that the area under the curve is equal to 1.

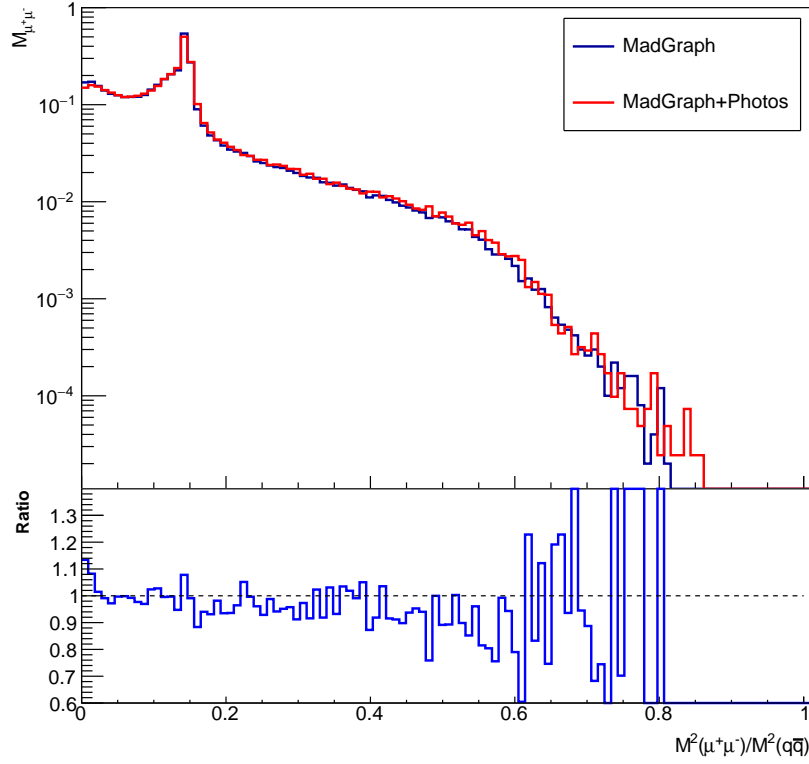


Fig. 5: The distribution of $\mu^+\mu^-$ invariant mass for $\sqrt{s} = 240$ GeV with all possible $\mu^+\mu^-$ pairs contributing (for each event four entries/combinations are added in the histogram). The upper panel shows the absolute distributions from the two generators, the lower panel shows the ratio of the two. The agreement is much better than what could have been deduced from Appendix B.3, where technical bias due to identical particles partial ordering was present.

duced with *MC-tester* difficult. That is why before it is invoked, the order of the muons in the event record is returned to its prior state before the call to the *Photos* interface. This has to be done to adopt to the *MC-tester* which recognizes the order of identical particles in the event record. The residual traces of the above arrangement are visible in the plots from appendices, but less so in Figs. 5 and 6 where the sum of the contributions from all $\mu^+\mu^-$ pairs is taken. The separation of phase space (with ± 3 GeV cut) into off- and on- Z peak regions helps but still migration of events from the Z peak to its side bands takes place. This exhibits as a peak in the ratio plot of Fig. 6. *Photos* algorithm can not simultaneously assure interferences of all Fig. 2 diagrams and Z peak phase space constraint. For that, complete 4-fermion and photon matrix element in emission kernel would be needed.

In order to answer the question how this translates into the ambiguities of observables used for the precision measurements requires use of observables that are (semi-)realistic from the detection point of view. To do it the prepared event samples (which were used for producing the presented plots), can be used.

Finally one may wonder about multi-photon effects. These can be implemented with *Photos* too and no further ambiguity should be expected, because the same emission kernel is then used.

3.1.3 $q\bar{q} \rightarrow \tau^+\tau^-\tau^+\tau^-(\gamma)$ at $\sqrt{s} = 10.5$ GeV

Finally, we have performed comparison between *MadGraph* and *Photos* final state bremsstrahlung for the process $q\bar{q} \rightarrow \tau^+\tau^-\tau^+\tau^-$ which will work in exactly the same way for the $e^+e^- \rightarrow \tau^+\tau^-\tau^+\tau^-$ process but is easier to initialize in *MadGraph*. In this case, τ leptons are moderately relativistic and terms proportional to τ mass are of importance, on the other hand contribution of the Z boson interaction is negligible. The study of *Photos* performance in such very different regime can be instructive. It may be of potential interest for Belle II phenomenology [22], that is why we have chosen the center of mass energy to be 10.5 GeV.

With the default version of *Photos* the agreement at the level of a factor of two was obtained. Clearly the mass terms of the 5-body system for τ leptons and photon final state are needed. It was relatively easy to introduce the necessary adjustment with the additional factor $(1 - 4m_\tau/\sqrt{s} - E_\gamma/\sqrt{s})^2$ for the internal *Photos* weight, resulting in softening of the photon energy spectrum. Such an ad hoc factor, can not replace a study of the matrix element but it can be assumed as an educated guess that represents its dominant, missing in this case, part. In fact, that is supported by the results of Fig. 7 which shows a very good agreement with the *MadGraph* calculation using exact matrix elements. Even though the obtained numerical results are encouraging such hypothesis require more rigorous study. In case of plots from Fig. 7 no kinematic cuts, except minimal

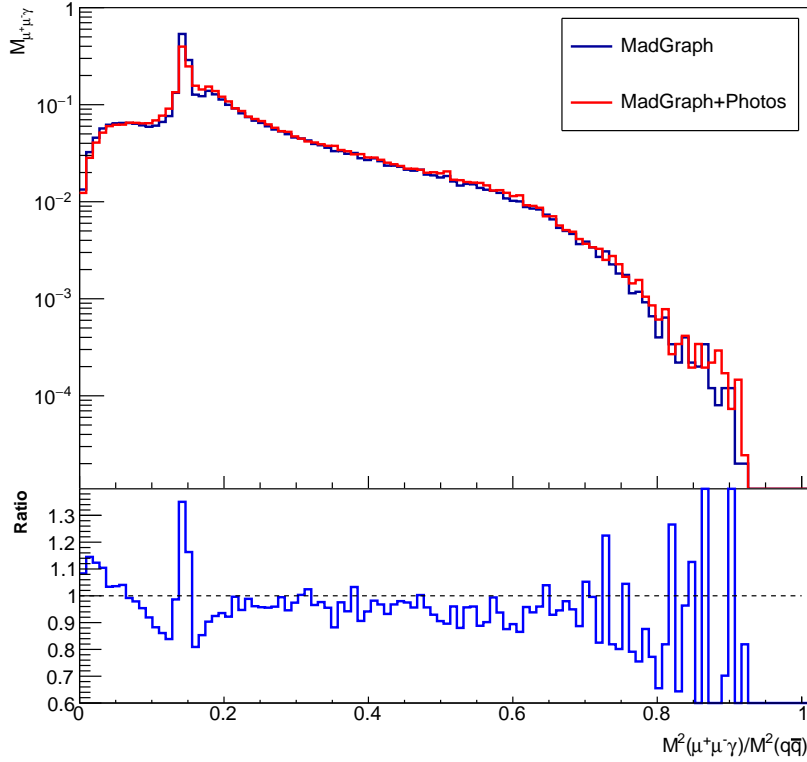


Fig. 6: The distribution of $\mu^+\mu^- \gamma$ invariant mass for $\sqrt{s} = 240$ GeV with all possible $\mu^+\mu^-$ pairs contributing (for each event four entries/combinations are added in the histogram). The upper panel shows the absolute distributions from the two generators, the lower panel shows the ratio of the two. The agreement is much better than what could have been deduced from Appendix B.3, where technical bias due to identical particles partial ordering was present. Note events migration from the Z peak to side bands. This is due to approximations in *Photos* kernel, for details see the text.

photon energy of 0.2 GeV, were applied. In Fig. 7 we can see that, compared to the analogous distributions for the four muon case at higher energies (e.g. in Fig. 6 and figures from Apps. B.1-B.3), the mass of τ lepton provides a clear cut-off at low $M^2(\gamma\tau\tau)$. Also we no longer see any remnants of the Z -peak.

3.2 Case of $\gamma\gamma \rightarrow l^+l^-(\gamma)$

Let us turn our attention to $\gamma\gamma \rightarrow e^+e^-(\gamma)$ that is a building block for some pp simulation programs. From technical side this case is simpler because incoming partons are not charged, and if one works in $\gamma\gamma$ collision frame, the $\gamma\gamma \rightarrow e^+e^-$ angular distribution does not peak. This may not be the case once strong boost to lab frame takes place.

The consequence of boost requires attention, especially for the cases when there are initial-state high p_T jets present. That may require detailed explanation and broader windows of generations of $\gamma\gamma \rightarrow l^+l^-$ samples than acceptance, as well as checks of the impact from the cuts in combinations with boosts. Note that *Photos* will “kick” some of the events into acceptance region and this need to be checked. It may be especially important for the multi-photon bremsstrahlung configurations.

On the other hand, nothing like that seems to be challenging from the perspective of our test runs, see Fig. 8. The obtained distributions are smooth and thanks to the used approximations

Photos works well. One should remember that collinear and soft photon phase space regions are excluded, but all hard non-collinear photon configurations are taken into account. That is the phase space region where *Photos* is not guaranteed to work well due to its design. Still, only for hardest emission sub-region which is scarcely populated, differences may approach 70%. That should be expected, as the kernel in *Photos* is not improved with matrix element for this case. The overall agreement between *Photos* and *MadGraph* is at the level of 0.01×0.05 , but at present this is from simplistic/naive tests only. The diagrams used for spin amplitudes are rather simple in this case, see Fig. 4.

To enable *Photos* activation we had to introduce intermediate cluster formed by the incoming $\gamma\gamma$ pair and then decaying to lepton pair.

4 Usage for phenomenology

In the previous parts of the paper we have explained the interface of *Photos* to our test environment (including *MadGraph*, *MC-tester* and *Photos* working in a single emission mode). This might have look complicated and hard to reproduce, but in usual applications, when it is not necessary to manipulate event record content, it is straightforward, see program manual [4]. As long as the events, for which the bremsstrahlung is to be added,

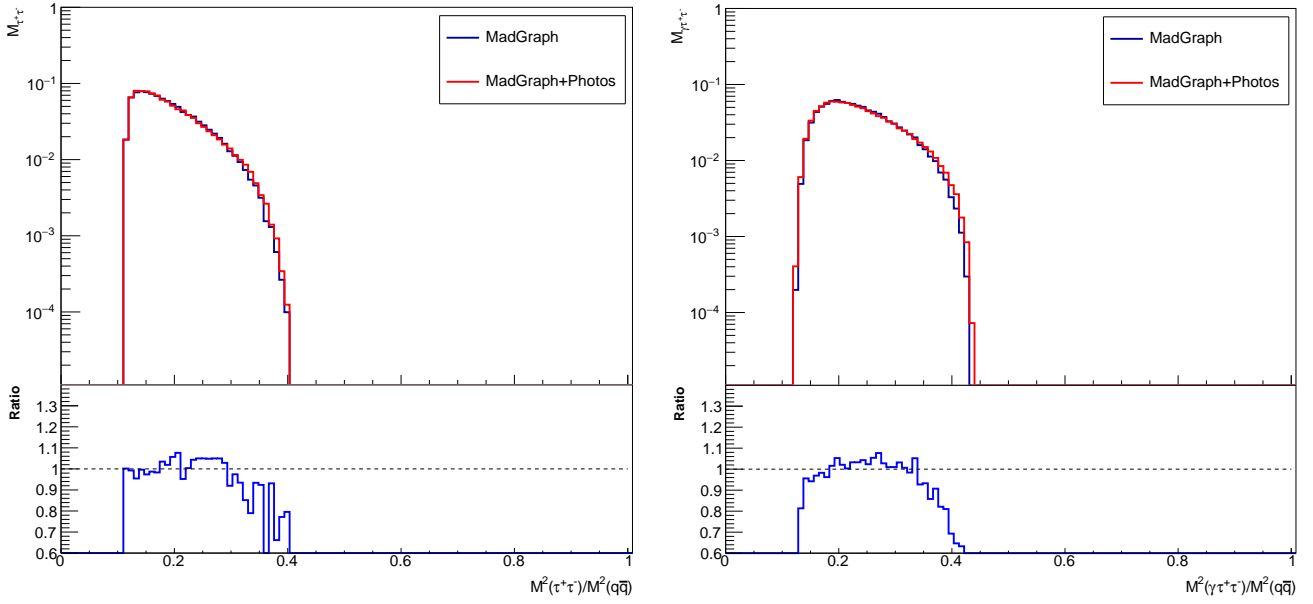


Fig. 7: The distributions of invariant mass of $\tau^+\tau^-$ (left panel) and $\tau^+\tau^-\gamma$ (right panel) for the $q\bar{q} \rightarrow \tau^+\tau^-\tau^+\tau^-$ process at $\sqrt{s} = 10.5$ GeV with $E_\gamma > 0.2$ GeV. The upper panel shows the absolute distributions from the two samples generated using MadGraph and MadGraph + Photos; the lower panel shows the ratio of the two.

are stored in HepMC [23] or Hepvt [24] format, we simply feed them to *Photos* and obtain back events of the same format but possibly with additional photons added. Such events can be further processed, e.g. by simulation of detector response. That is why *Photos* can work with any generator chain, without any burden for the user.

Our paper explains reliability tests of *Photos* for events with hard non-collinear photons where it may not be accurate. For comparison with MadGraph simulation where single photon configurations are generated from exact phase space and exact matrix element, also the *Photos* single photon mode of operation has to be activated. In practice, *Photos* is expected to be used in the multi-photon mode covering the whole phase space also that of collinear and soft photons. *Photos* algorithm is closely related to exponentiation, that is why, e.g. the Yennie-Frautschi-Suura β_1 part [25–28] of the second order matrix element is taken into account.

We note that a full scale matching of *Photos* with higher order matrix element for $q\bar{q} \rightarrow 4l + \gamma$ like processes would require development of a dedicated matching scheme. Preferably separating matrix element into parts corresponding to Born times eikonal factor and the so-called β_1 of Yennie Frautschi Suura exponentiation. Unfortunately it requires major effort. Separation of the phase space into soft photon region, for which *Photos* would be used like in [29] and matrix element generator for hard emissions is also possible, but again would require considerable effort. For the moment we have demonstrated that using an approximate treatment provided by *Photos* gives sufficiently good results for many current applications.

5 Summary

In the paper, we have addressed the question of how reliable is using *Photos* Monte Carlo for simulation of final state bremsstrahlung in $e^+e^-(q\bar{q}) \rightarrow l^+l^-l^+l^-$ and $\gamma\gamma \rightarrow l^+l^-(n\gamma)$ hard processes. *Photos* algorithm is prepared for combination with complete simulation chain (as used in experimental analyses) and is expected to be used as an add up solution for bremsstrahlung in decay of particles or resonances. The applicability of *Photos* extends beyond processes selected here. Evaluation of ambiguities is thus of particular importance, especially if hard and/or non-collinear photon emissions are of interest. For such configurations comparisons with matrix element tree-level based simulation was now performed; *Photos* operation was restricted to single photon emissions only. Then full phase space with explicit parametrization was used and the differences with respect to reference MadGraph simulations are shown. In this way approximations used in *Photos* emission kernel (its simplified matrix element) are exposed. The comparisons relied on automatically defined and collected 1-dimensional distributions of all possible invariant masses which can be constructed from the outgoing particles. These full results are collected in the Appendices, whereas in Sec. 3 selected results of particular interest were recalled. Only the events with hard non-collinear photons were taken into account because that is the phase space region where source of ambiguities is expected to reside. For the soft or collinear photons *Photos* algorithm is expected to work in a general case.

The obtained agreement level is encouraging. We quantify it as the difference between area under the invariant mass histograms, and in all considered cases such differences are below 3%. Note that monitored events represented up to 10% of the samples for the selected processes and cuts. In this way, we can indicate size of the ambiguities due to the approxima-

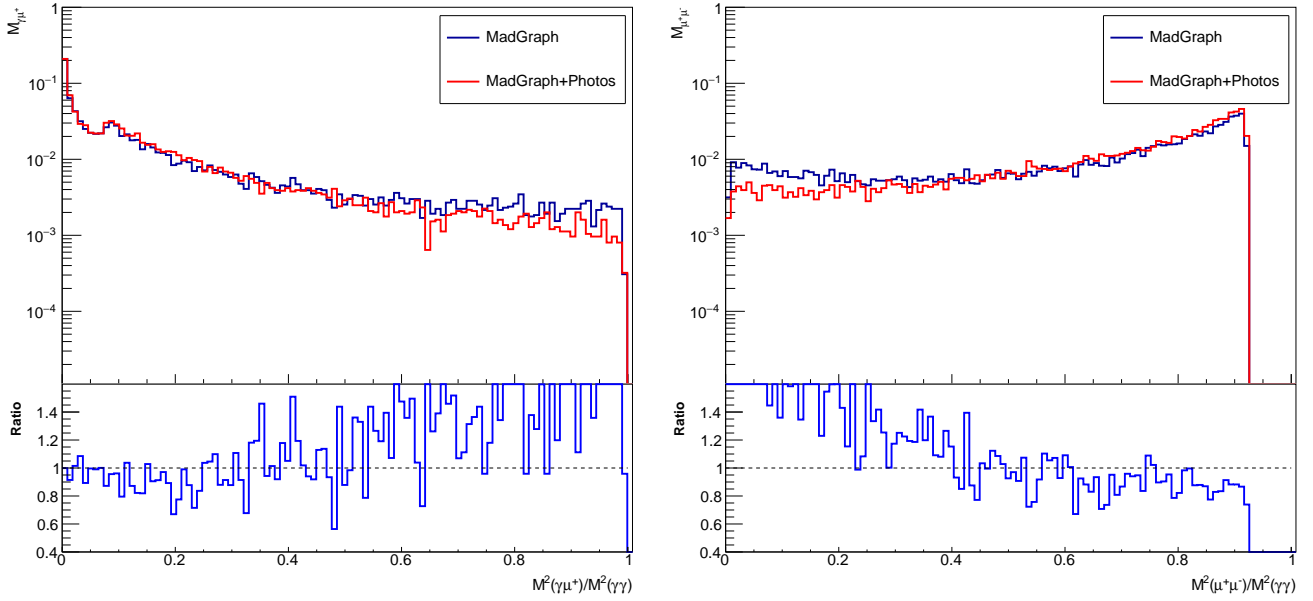


Fig. 8: The distribution of invariant mass of $\mu^+\gamma$ (left panel) and $\mu^-\mu^+\gamma$ (right panel) for the $\gamma\gamma \rightarrow \mu^-\mu^+\gamma$ process. Comparison between *Photos* and MadGraph. For details of selection cuts see the text. Collinear and soft photon phase space regions are excluded, but all hard non-collinear photon configurations are taken into account. That is the phase space region where *Photos* is not guaranteed to work well due to its design. Still, only for hardest emission sub-region which is scarcely populated, differences may approach 70%. That should be expected, as the kernel in *Photos* is not improved with matrix element for this case.

tions used in *Photos*. Similar reliability for further processes also somewhat outside of *Photos* applicability range can be expected.

Naively one could take the size of the obtained differences ($\sim 3\%$) and the fact that approximations affect only subset of actual events ($\sim 10\%$) to estimate the global effect as $3\% * 10\%$ thus giving 0.003. For $\gamma\gamma \rightarrow \mu^+2\mu^-(\gamma)$ agreement seem to be even better. Once these tests are completed we can address effects of multi-photon radiation. This can be taken into account with the help of bremsstrahlung photon simulation segment of *Photos*. Full simulation chains is then enriched, without much of intervention into the software design. However, since we have not used realistic or even idealized observables to evaluate the impact of approximation on observables of phenomenological interest, we can not claim that precision with certainty. For that, additional work using dedicated event samples and idealized observables is needed and we are looking forward to such work.

One should stress that *Photos* was not expected to be used for processes with strong t -channel transfer dependence or for processes where non-bremsstrahlung matrix elements vary largely over the phase space, e.g. due to intermediate resonances. This required special attention. E.g. if the intermediate Z -boson resonances were explicitly written into the content of event records, prior to invoking *Photos*, allowed to reduce the differences, especially for the cases of $2\mu^+2\mu^-$ and $\mu^+\mu^-l^+l^-$ production at 240 GeV.

Acknowledgments

This project was supported in part from funds of Polish National Science Centre under decisions DEC-2017/27/B/ST2/01391.

Encouragement from the Polish-French collaboration no. 10-138 within IN2P3 through LAPP Annecy and during the years leading to completion of this work is also acknowledged.

References

1. E. Richter-Was and Z. Was, “Adequacy of Effective Born for electroweak effects and TauSpinner algorithms for high energy physics simulated samples,” *Eur. Phys. J. Plus* **137** no. 1, (2022) 95, [arXiv:2012.10997 \[hep-ph\]](#).
2. C. Gütschow and M. Schönherr, “Four lepton production and the accuracy of QED FSR,” *Eur. Phys. J. C* **81** no. 1, (2021) 48, [arXiv:2007.15360 \[hep-ph\]](#).
3. E. Barberio and Z. Was, “Photos: A universal monte carlo for qed radiative corrections. version 2.0,” *Comput. Phys. Commun.* **79** (1994) 291–308.
4. N. Davidson, T. Przedzinski, and Z. Was, “PHOTOS interface in C++: Technical and Physics Documentation,” *Comput. Phys. Commun.* **199** (2016) 86–101, [arXiv:1011.0937 \[hep-ph\]](#).
5. J. Alwall, R. Frederix, S. Frixione, V. Hirschi, F. Maltoni, O. Mattelaer, H. S. Shao, T. Stelzer, P. Torrielli, and M. Zaro, “The automated computation of tree-level and next-to-leading order differential cross sections, and their matching to parton shower simulations,” *JHEP* **07** (2014) 079, [arXiv:1405.0301 \[hep-ph\]](#).
6. J. M. Campbell, R. K. Ellis, and C. Williams, “Vector boson pair production at the LHC,” *JHEP* **07** (2011) 018, [arXiv:1105.0020 \[hep-ph\]](#).
7. J. Campbell and T. Neumann, “Precision Phenomenology with MCFM,” *JHEP* **12** (2019) 034, [arXiv:1909.09117 \[hep-ph\]](#).
8. T. Melia, P. Nason, R. Rontsch, and G. Zanderighi, “ $W+W-$, WZ and ZZ production in the POWHEG BOX,” *JHEP* **11** (2011) 078, [arXiv:1107.5051 \[hep-ph\]](#).

9. S. Alioli, P. Nason, C. Oleari, and E. Re, “A general framework for implementing NLO calculations in shower Monte Carlo programs: the POWHEG BOX,” *JHEP* **06** (2010) 043, [arXiv:1002.2581 \[hep-ph\]](#).
10. F. Cascioli, S. Höche, F. Krauss, P. Maierhöfer, S. Pozzorini, and F. Siegert, “Precise Higgs-background predictions: merging NLO QCD and squared quark-loop corrections to four-lepton + 0,1 jet production,” *JHEP* **01** (2014) 046, [arXiv:1309.0500 \[hep-ph\]](#).
11. T. D. Lee and M. Nauenberg, “Degenerate Systems and Mass Singularities,” *Phys. Rev.* **133** (1964) B1549–B1562.
12. T. Kinoshita, “Mass singularities of Feynman amplitudes,” *J. Math. Phys.* **3** (1962) 650–677.
13. P. Golonka and Z. Was, “PHOTOS Monte Carlo: A Precision tool for QED corrections in Z and W decays,” *Eur. Phys. J. C* **45** (2006) 97–107, [arXiv:hep-ph/0506026](#).
14. G. Nanava and Z. Was, “Scalar QED, NLO and PHOTOS Monte Carlo,” *Eur. Phys. J. C* **51** (2007) 569–583, [arXiv:hep-ph/0607019](#).
15. E. Richter-Was, “Hard photon bremsstrahlung in the process $p p \rightarrow Z0 / \gamma^* \rightarrow \text{lepton} + \text{lepton}$: A background for the intermediate mass Higgs,” *Z. Phys.* **C64** (1994) 227–240.
16. P. Golonka and Z. Was, “Next to leading logarithms and the PHOTOS Monte Carlo,” *Eur. Phys. J. C* **50** (2007) 53–62, [arXiv:hep-ph/0604232](#).
17. G. Nanava, Q. Xu, and Z. Was, “Matching NLO parton shower matrix element with exact phase space: Case of $W \rightarrow l \nu(\gamma)$ and $\gamma^* \rightarrow \pi^+ \pi^-(\gamma)$,” *Eur. Phys. J. C* **70** (2010) 673–688, [arXiv:0906.4052 \[hep-ph\]](#).
18. N. Davidson, P. Golonka, T. Przedzinski, and Z. Was, “MC-TESTER v. 1.23: a universal tool for comparisons of Monte Carlo predictions for particle decays in high energy physics,” *Comput. Phys. Commun.* **182** (2011) 779–789, [arXiv:0812.3215 \[hep-ph\]](#).
19. S. Antropov, A. Arbuzov, R. Sadykov, and Z. Was, “Extra lepton pair emission corrections to Drell-Yan processes in PHOTOS and SANC,” *Acta Phys. Polon. B* **48** (2017) 1469, [arXiv:1706.05571 \[hep-ph\]](#).
20. S. Antropov, “High Precision Lepton Pair Bremsstrahlung with PHOTOS,” *Acta Phys. Polon. B* **51** no. 6, (2020) 1221–1229.
21. S. Jadach, M. Skrzypek, and B. F. L. Ward, “Soft pairs real and virtual infrared functions in QED,” *Phys. Rev. D* **49** (1994) 1178–1182.
22. Belle-II Collaboration, L. Aggarwal *et al.*, “Snowmass White Paper: Belle II physics reach and plans for the next decade and beyond,” [arXiv:2207.06307 \[hep-ex\]](#).
23. M. Dobbs and J. B. Hansen, “The HepMC C++ Monte Carlo event record for High Energy Physics,” *Comput. Phys. Commun.* **134** (2001) 41–46. <https://savannah.cern.ch/projects/hepmc/>.
24. G. Altarelli, R. Kleiss, and C. Verzegnassi, eds., *Z physics at LEP-I. Proceedings, Workshop, Geneva, Switzerland, September 4-5, 1989. vol. 1: Standard Physics*. 1989. <http://inspirehep.net/record/288139/files/CERN-89-08-V-1.pdf>.
25. D. R. Yennie, S. Frautschi, and H. Suura *Ann. Phys. (NY)* **13** (1961) 379.
26. S. Jadach, W. Placzek, M. Skrzypek, B. F. L. Ward, and Z. Was *Phys. Lett.* **B417** (1998) 326.
27. S. Jadach, Z. Was, and B. F. L. Ward, “The precision monte carlo event generator *kkmc* for two-fermion final states in e^+e^- collisions,” *Comput. Phys. Commun.* **130** (2000) 260. Up to date source available from <http://home.cern.ch/jadach/>.
28. A. Arbuzov, S. Jadach, Z. Was, B. Ward, and S. Yost, “The Monte Carlo Program KKMC for the Lepton or Quark Pair Production at LEP/SLC Energies – updates of electroweak calculations,” *Comput. Phys. Commun.* **260** (2021) 107734, [arXiv:2007.07964 \[hep-ph\]](#).
29. L. Barze, G. Montagna, P. Nason, O. Nicrosini, F. Piccinini, and A. Vicini, “Neutral current Drell-Yan with combined QCD and electroweak corrections in the POWHEG BOX,” *Eur. Phys. J. C* **73** no. 6, (2013) 2474, [arXiv:1302.4606 \[hep-ph\]](#).

A Details on running `MadGraph` and kinematic cuts

Below we list the definitions of kinematic variables used when constructing kinematic cuts in Sec. 2.1 for the events in samples generated from `MadGraph` and later analyzed with addition of photon from `Photos`:

- Rapidity: $\eta = 0.5 \ln \left(\frac{p_t + p_z}{p_t - p_z} \right)$, with $p_t(p_z)$ being the zero (third) component of 4-momentum of given particle.
- Invariant mass of two particles: $m_{ab} = \sqrt{(p_a + p_b)^2}$, with p_a, p_b the 4-momenta of particle a and b .
- Distance between two particles a and b : $\Delta R_{ab} = \sqrt{(\eta_a - \eta_b)^2 + \Delta\phi_{ab}^2}$, with ϕ being the orientation angle (in radians) which is defined for the momenta components in the x - y plane which is perpendicular to the beam direction given by z , specifically we have: $\Delta\phi_{ab}^2 = \arccos \left(\frac{p_{ax}p_{bx} + p_{ay}p_{by}}{\sqrt{p_{ax}^2 + p_{ay}^2} \sqrt{p_{bx}^2 + p_{by}^2}} \right)$.
- Transverse energy: $E_t = \sum_{i \in \text{leptons}} \sqrt{(p_i^1)^2 + (p_i^2)^2}$.

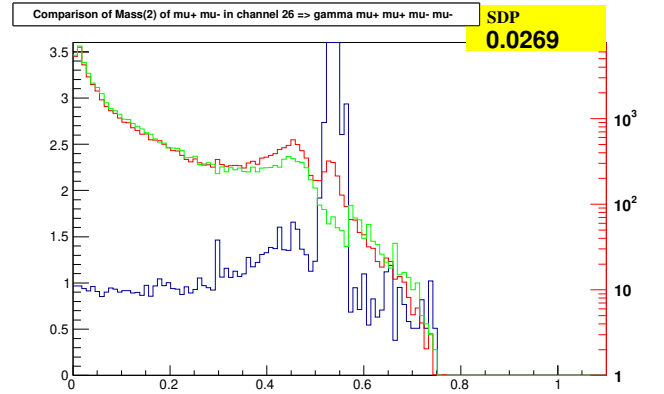
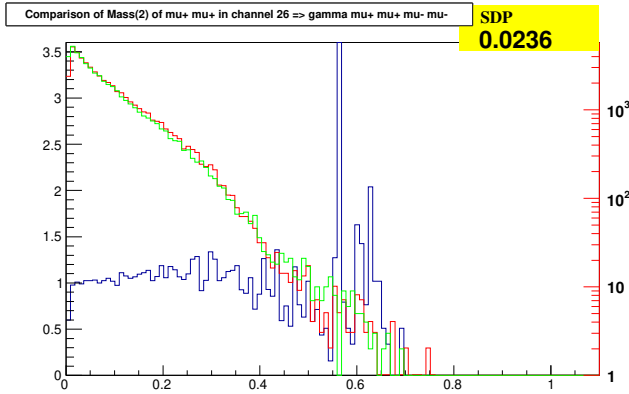
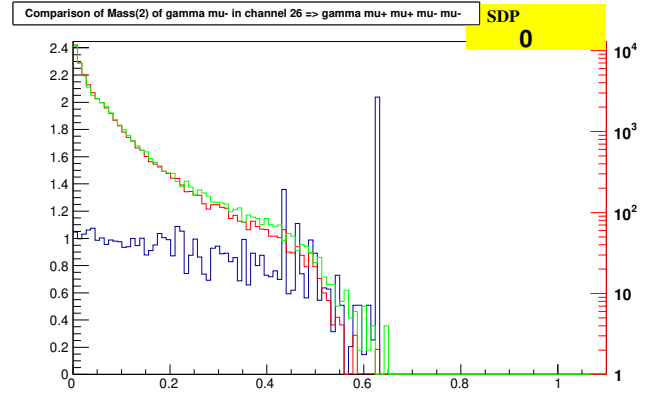
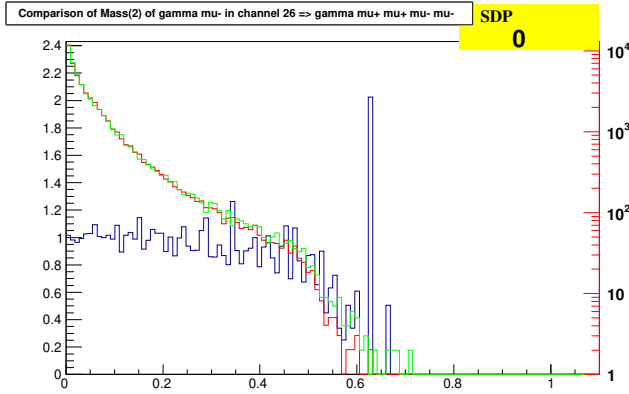
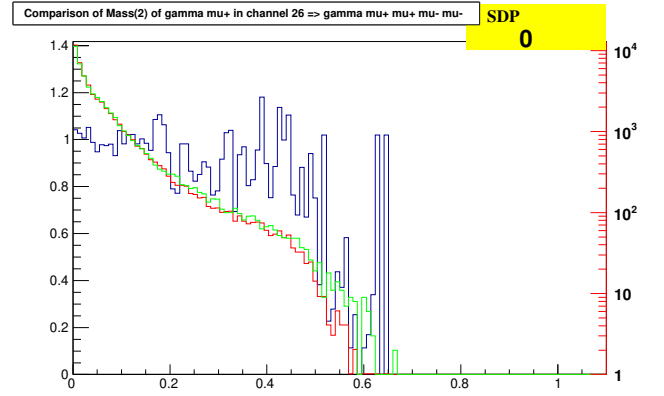
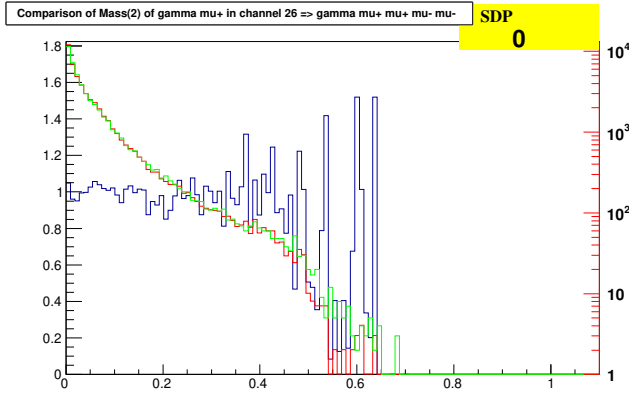
We also provide here an example input file (run card) for running `MadGraph` simulation for the $q\bar{q} \rightarrow l^+ l^- l^+ l^- \gamma$ process.

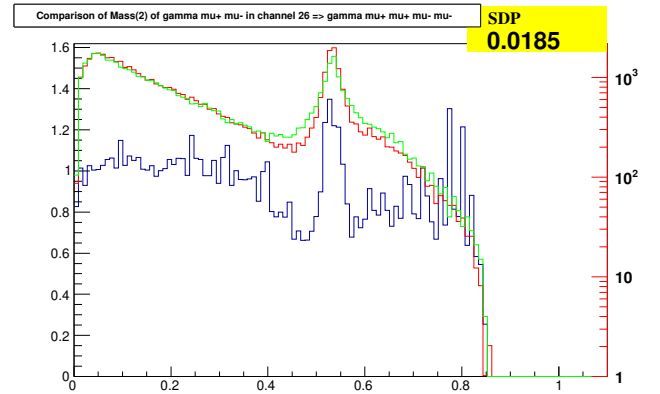
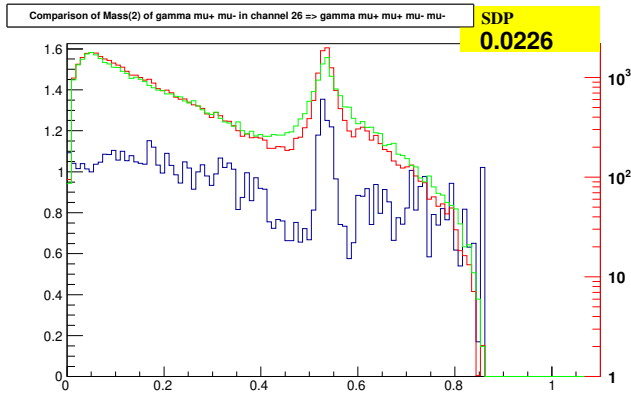
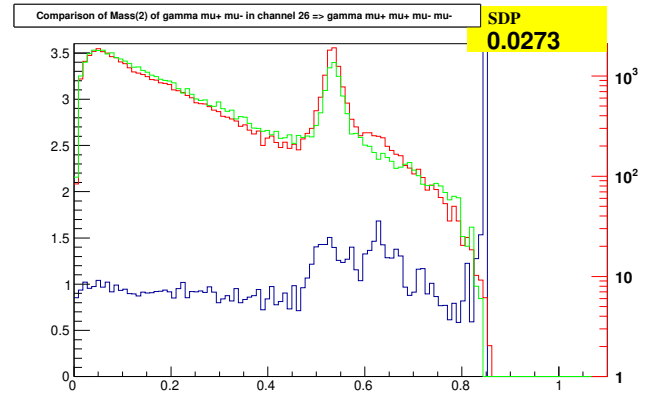
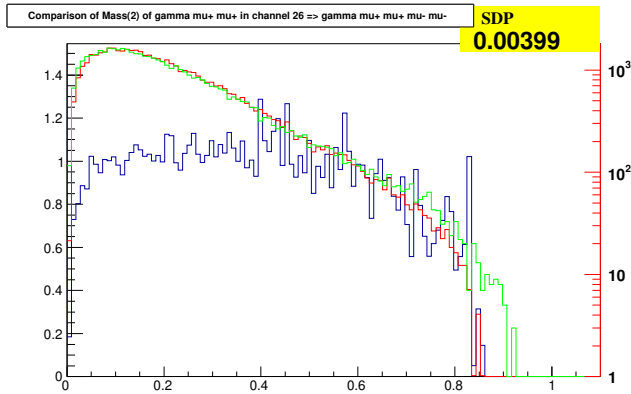
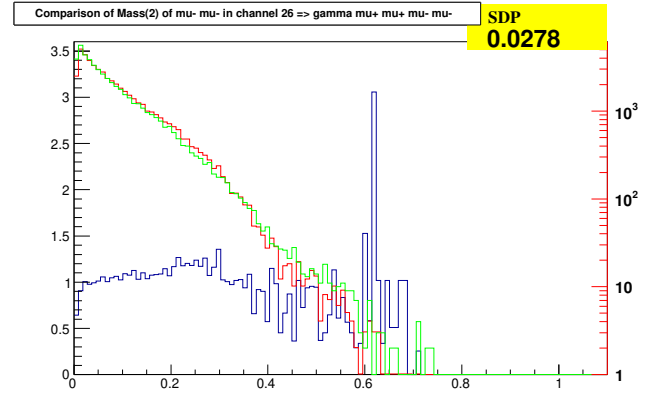
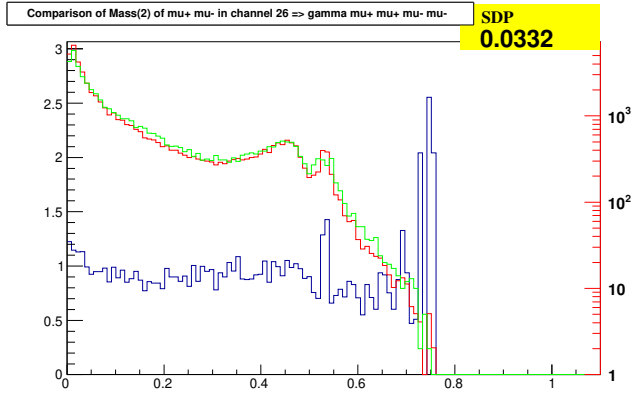
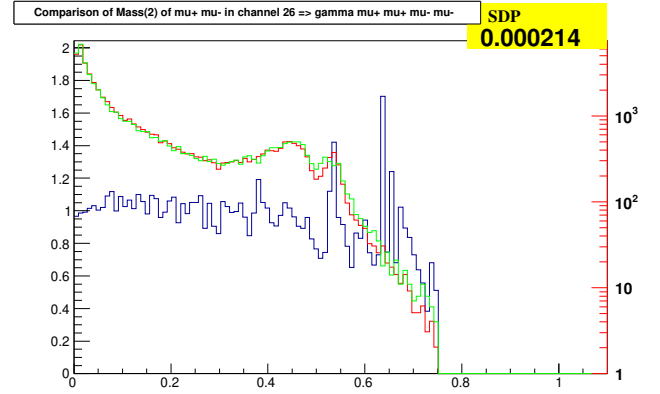
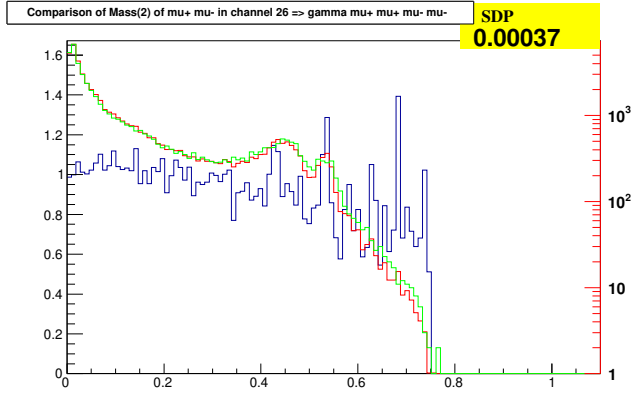
```
import model loop_sm-lepton_masses
generate p p > mu+ mu- mu+ mu- a QCD=0 QED=5 / h --diagram_filter
output FCC240_qq_4muA_Inc_QED5_noISR_500k
launch FCC240_qq_4muA_Inc_QED5_noISR_500k
analysis=off
set mta 0.10566
set ymtau 0.10566
set nevents 500k
set lpp1 0
set lpp2 0
set ebeam1 120.
set ebeam2 120.
set use_syst false
set no_parton_cut
set cut_decays true
set etal 3 # max rapidity of charged lepton
set etaa 3 # max rapidity of photons
set ea 5 # minimum E for the photons
set mml1 9 # minimal invariant mass of (same flavour) lepton pairs: l+l-
set eta_max_pdg {15:3, 13:3} # max eta for mu (13:) and tau (15:)
set mxx_min_pdg {15:9, 13:9} # min invariant mass of a pair of particles X/X~ (mu, tau)
set drll 0.4 # distance between leptons
set dral 0.4 # distance between gamma and lepton
set r0gamma 0.4
set xn 1
set isoEM true
set epsgamma 1.0
done
```

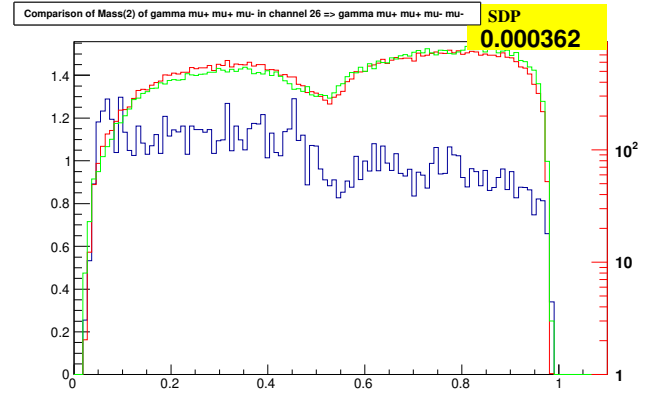
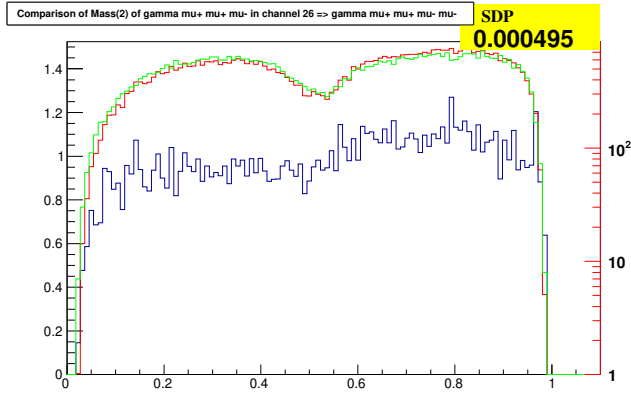
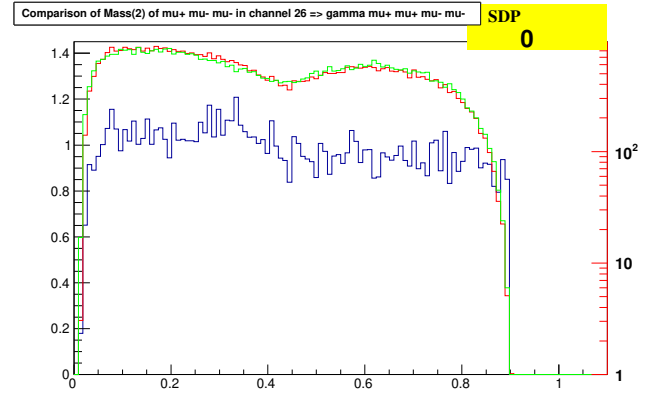
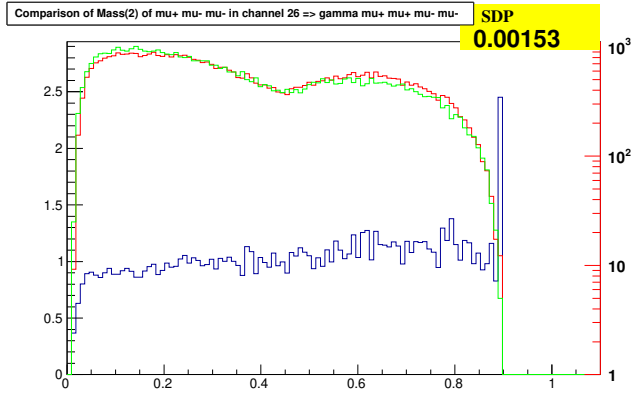
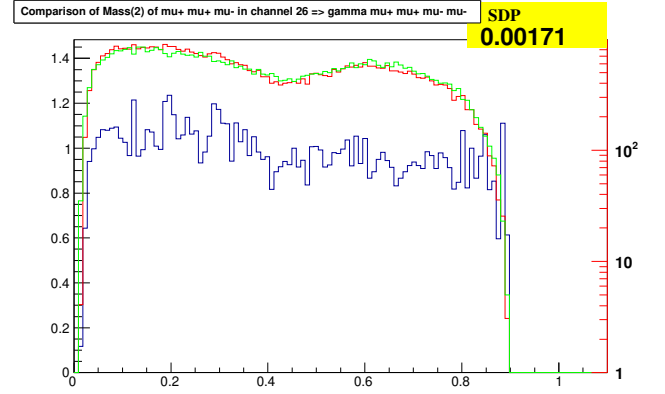
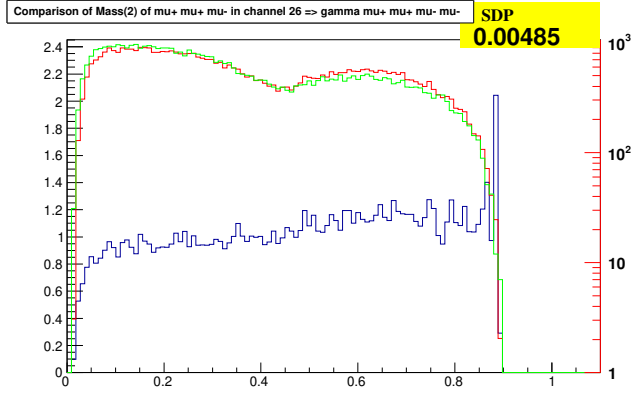
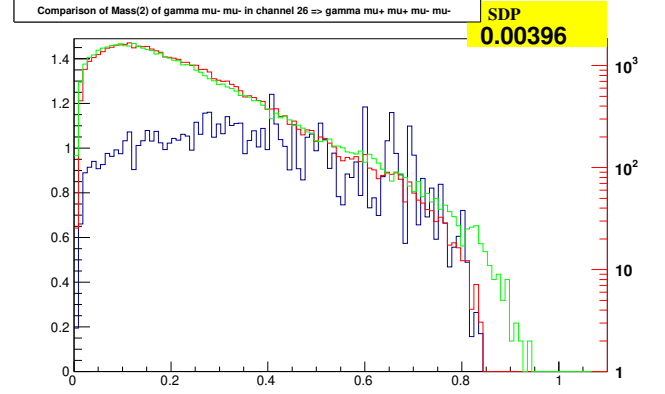
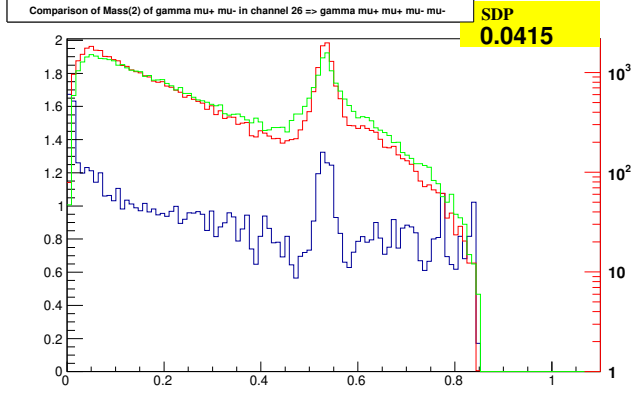
B Technical comparison plots for $q\bar{q} \rightarrow \gamma\mu^+\mu^-\mu^+\mu^-$ at different energies

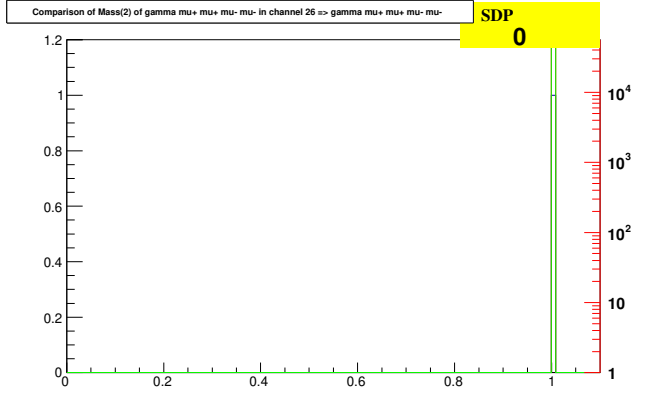
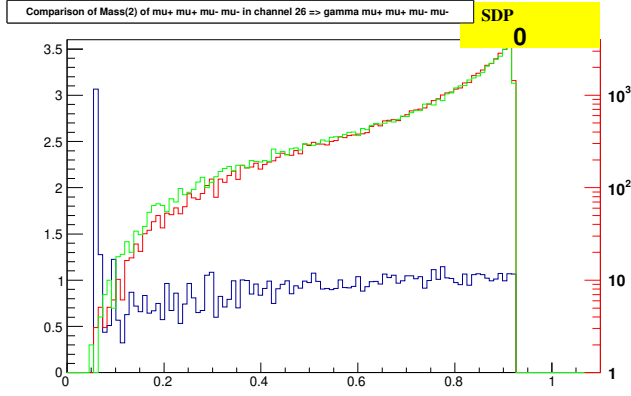
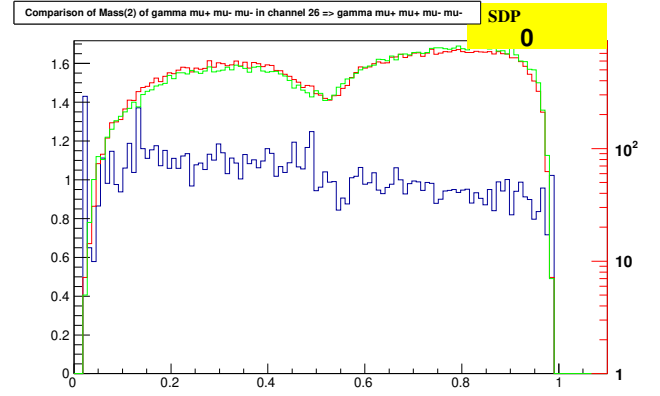
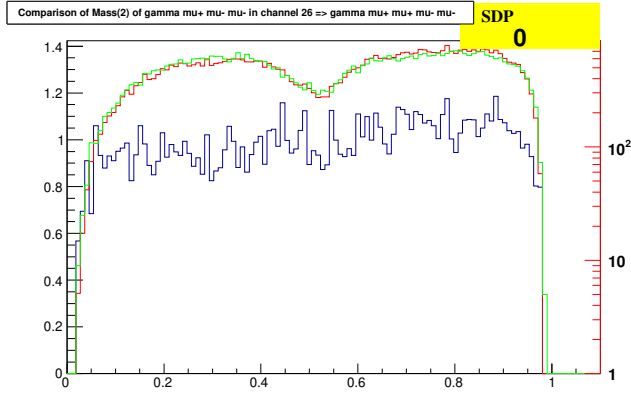
In appendices B.1-B.3 we present technical comparison plots for processes with production of four leptons at energies of 125-240 GeV that were discussed in Sec. 3.1. The plots display invariant mass distributions of all combinations of the final state particles produced either with *MadGraph* or with *MadGraph* plus *Photos*. The plots have two axes the right one gives the number of events and corresponds to the invariant mass distributions (plotted in green and red), the left one corresponds to the ratio of the two distributions (plotted in blue). All the plots were produced automatically using the *MC-tester* program [18]. Additionally in yellow box we display value of “SDP” which is the difference of the area under the normalized histograms of the distributions from the two generators which is used to judge the differences between the two generators. The details on the precise definition of “SDP” can be found in the program manual [4].

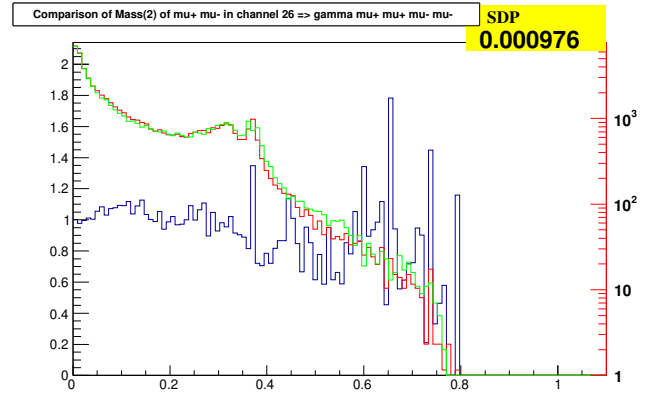
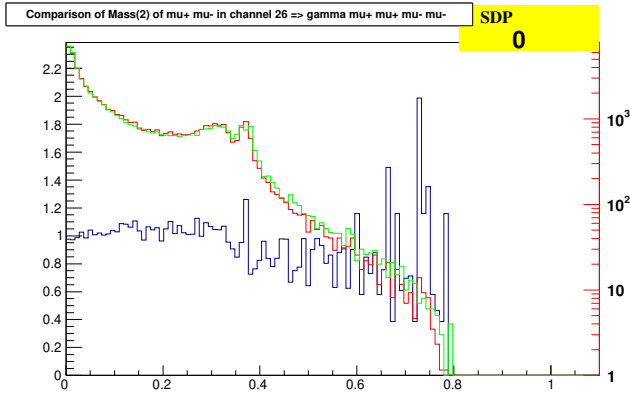
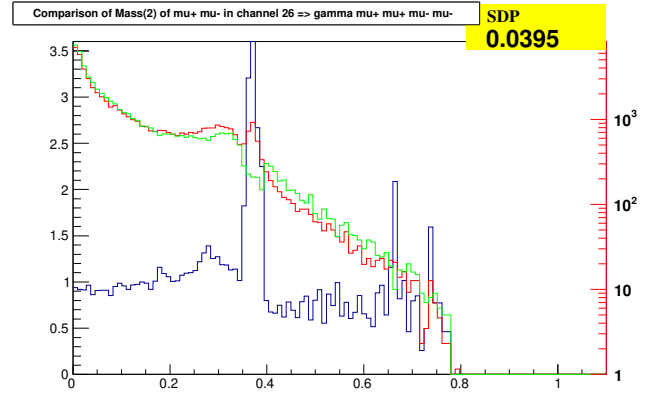
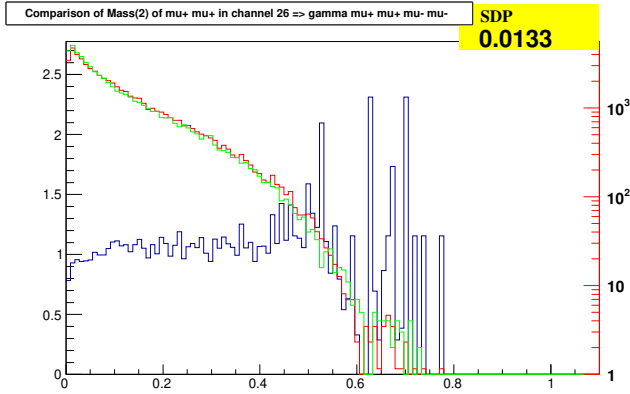
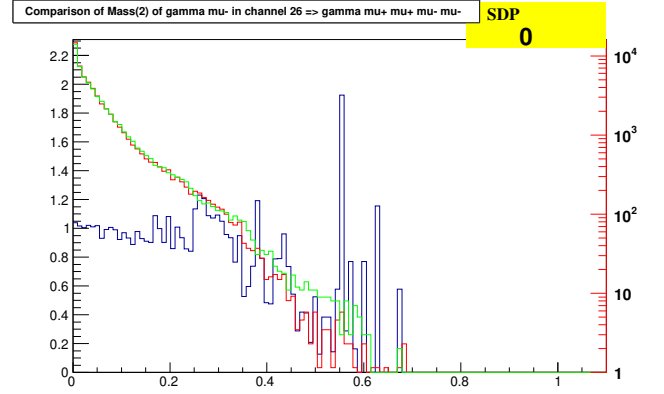
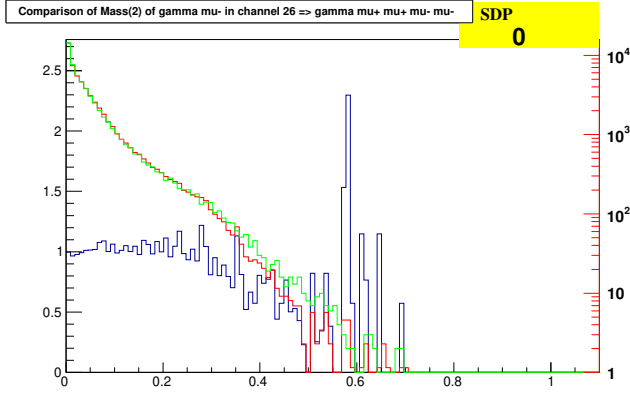
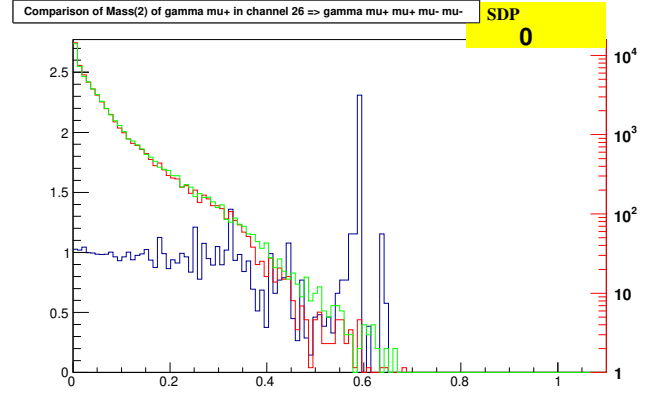
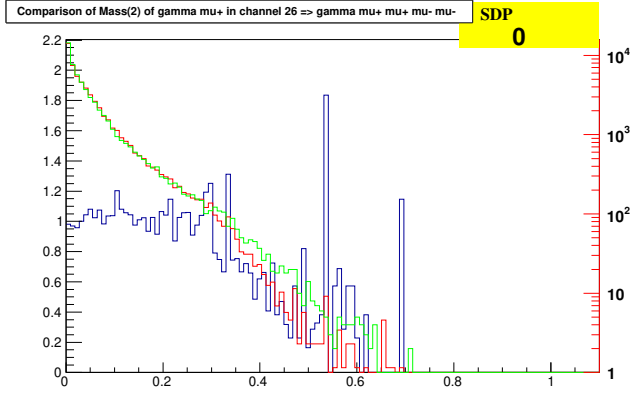
B.1 MC-tester: $q\bar{q} \rightarrow \gamma\mu^+\mu^-\mu^+\mu^-$ at $\sqrt{s} = 125$ GeV

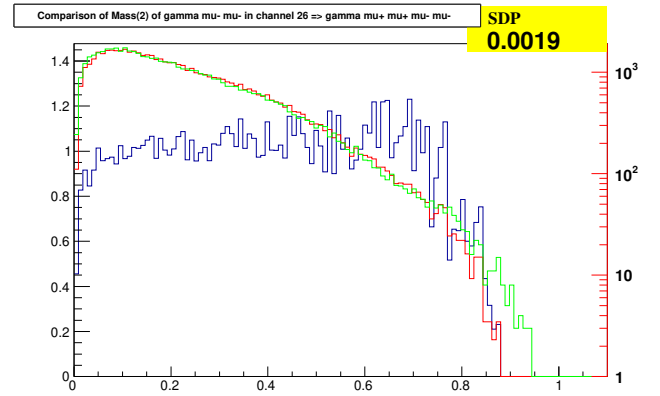
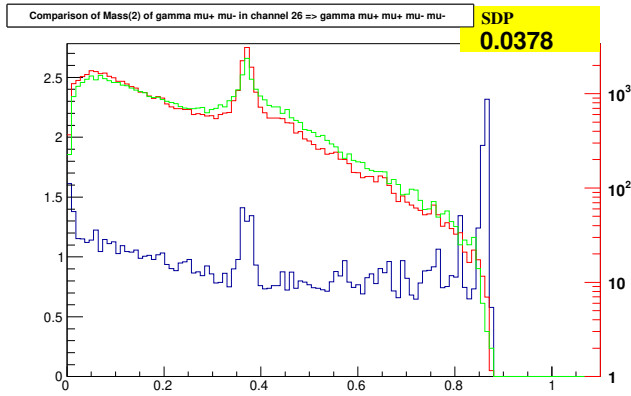
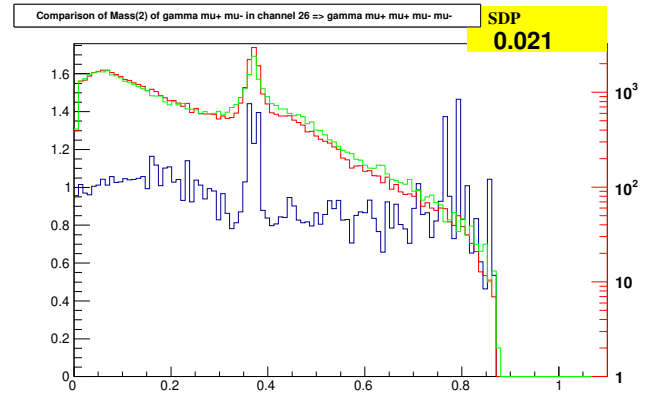
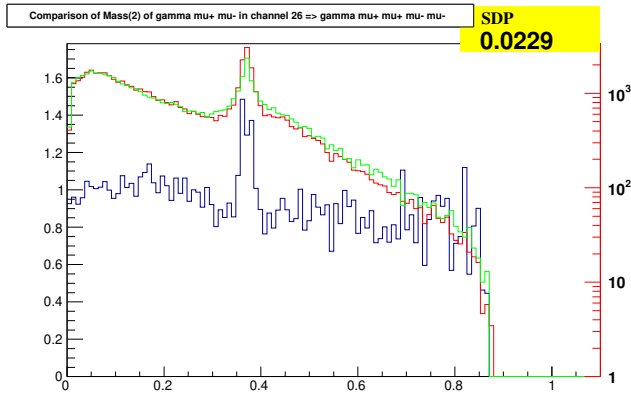
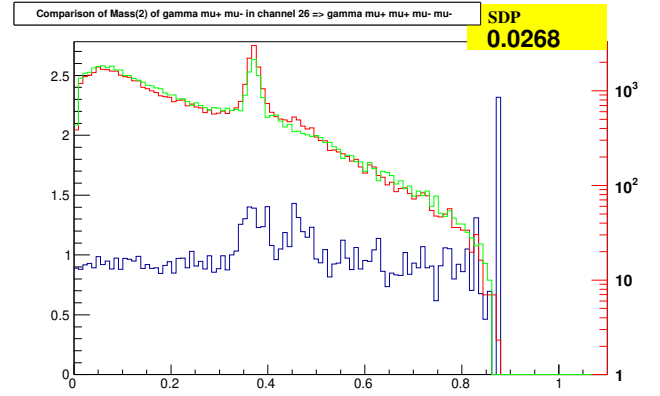
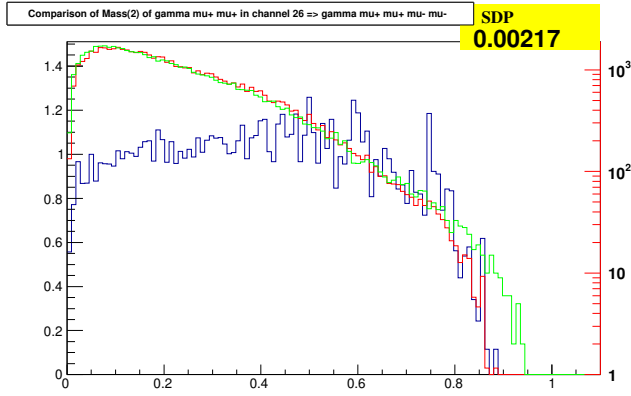
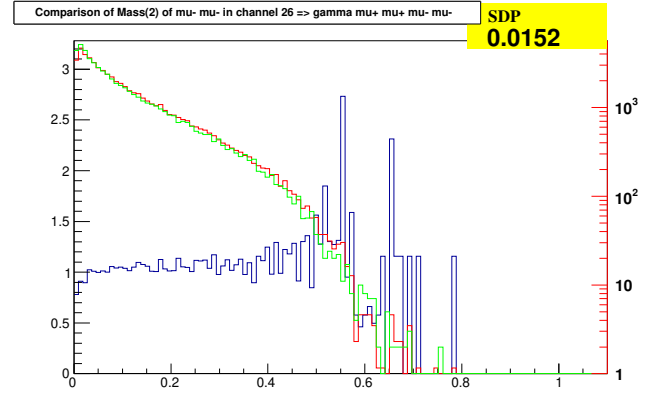
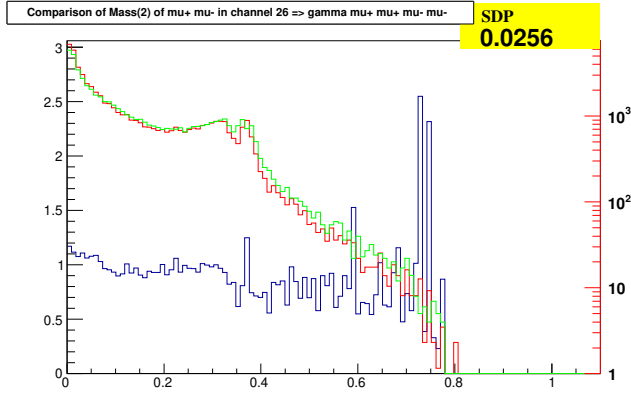


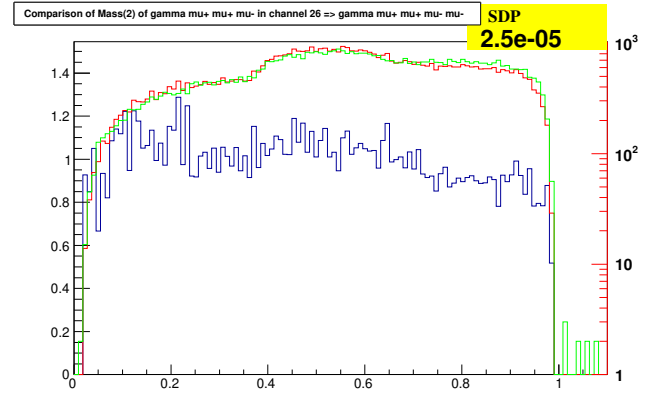
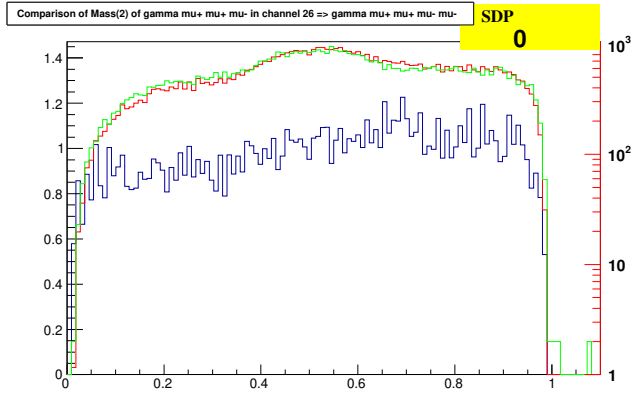
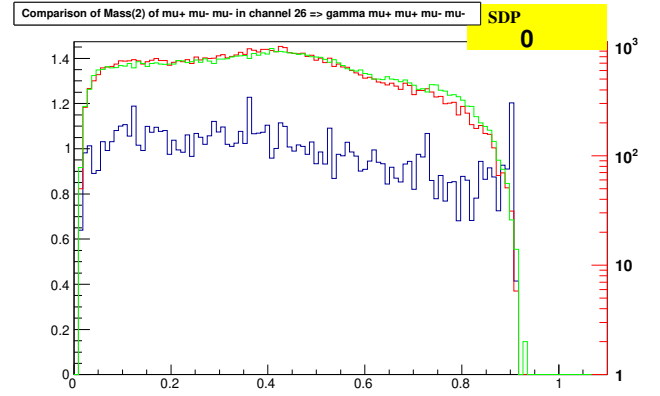
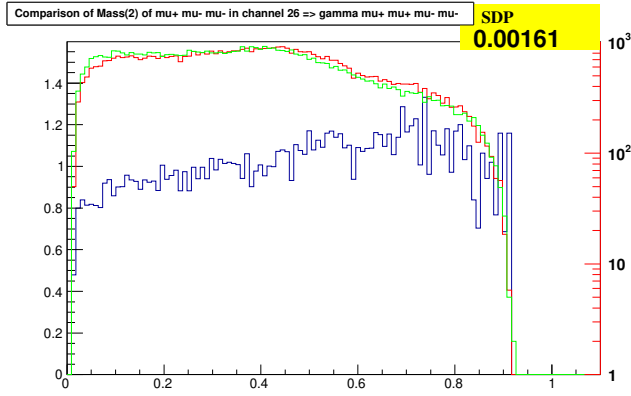
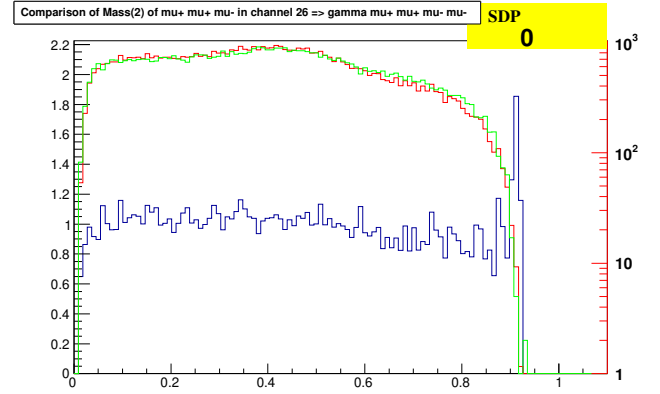
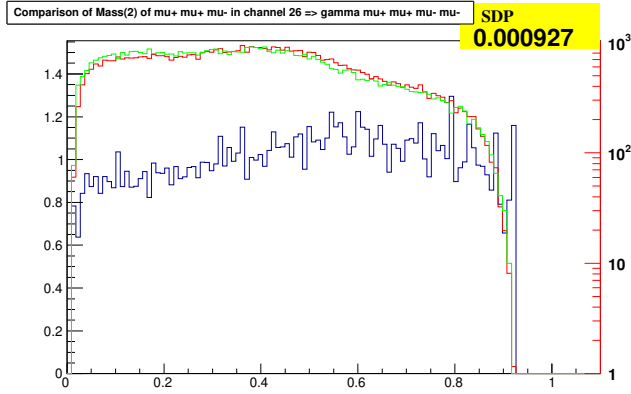


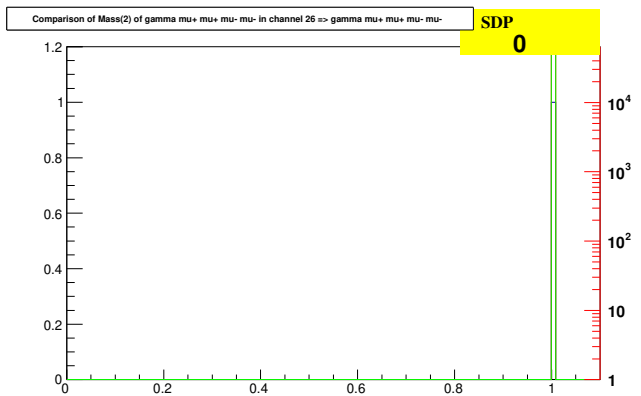
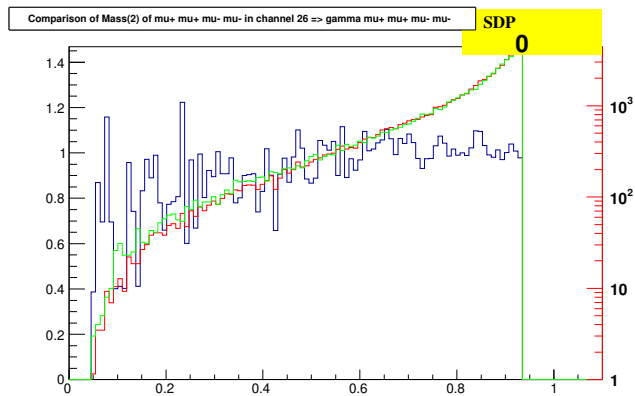
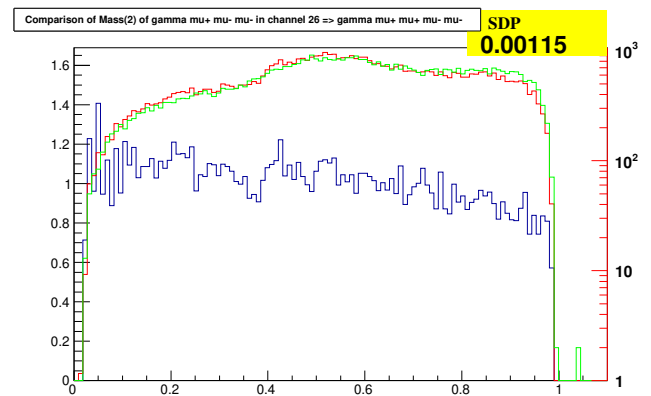
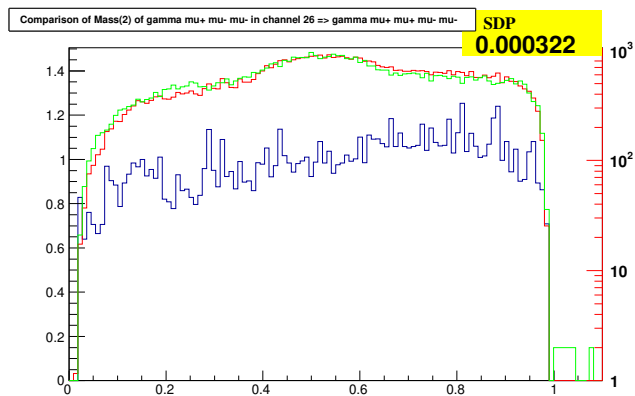




B.2 MC-tester: $q\bar{q} \rightarrow \gamma\mu^+\mu^+\mu^-\mu^-$ at $\sqrt{s} = 150$ GeV







B.3 MC-tester: $q\bar{q} \rightarrow \gamma\mu^+\mu^+\mu^-\mu^-$ at $\sqrt{s} = 240$ GeV